

Hadronic- and electromagnetic-cores of air-showers observed by hybrid experiments at high mountains

M.Tamada

Faculty of Science and Engineering, Kinki University, Higashi-Osaka, 577-8502 Japan

Characteristics of the high energy families (bundle of high energy e, γ) and hadrons in the air-showers detected in the hybrid experiment together with emulsion chamber and AS-array at Mt.Chacaltaya are studied in detail by comparing with those of CORSIKA simulations using interaction models of QGSJET and EPOS. Because the atmospheric families and hadron component have more direct information of the nuclear interaction, correlations between atmospheric families and burst (hadron component of air-showers) accompanied to air-showers are more sensitive to the mechanism of the cosmic-ray interactions. The burst size dependence of the family energy is compared with those of simulations. It is found that the family energy accompanied by the air-showers with the larger burst-size is systematically smaller than that expected in the simulated events. The experimental results can not be described simply by changing the chemical composition of primary cosmic-rays and this indicates that the x-distribution of secondary particles in cosmic-ray interactions becomes much steeper than that assumed in the simulation models.

1. Introduction

The main interests of the cosmic-ray study now shift to the highest energy region, $E_0 \geq 10^{19}$ eV, using huge experimental apparatus to search for astrophysical sources and the acceleration or emission mechanism of those extreme high energy cosmic-rays. However, half a century after its discovery, the “knee” in the cosmic-ray spectrum, a steepening of the energy spectrum at $10^{15} \sim 10^{16}$ eV, is still not well understood. Because of the low intensities, direct observations of primary cosmic-rays in this energy range are still not possible and so various types of air-shower experiments at high mountains and also at ground level have been carried out in order to investigate the chemical composition of primary cosmic-rays in this energy region which gives important information on the physical origin of cosmic-rays [1–7]. The experimental data in those indirect measurement are usually interpreted by comparing with Monte Carlo simulations assuming some models of cosmic-ray interactions. Many experimental groups claim that the fraction of heavy primaries increases rapidly beyond the “knee” region, e.g., the fraction of protons is estimated by the Tibet AS- γ group [8] to be as small as $\sim 10\%$ of all particles for $E_0 = 10^{15} - 10^{16}$ eV. The results, however, depend on their assumed interaction model. For example, the EPOS model recently proposed [9, 10] gives muon numbers much more than the QGSJET model. The events which can be interpreted due to heavy primary when we employ the QGSJET model as nuclear interactions are interpreted due to proton primaries when EPOS is used as the interaction model [11]. Thus the interpretations rely heavily on the Monte Carlo calculations. In fact, various experimental groups give various data on chemical composition in this energy region and the results are still very confusing. We should examine whether the overall experimental data can be well interpreted by the

assumed model before drawing a conclusion.

Hybrid experiments operating simultaneously an air-shower array, a hadron calorimeter and an emulsion chamber have been carried out at Mt. Chacaltaya (5200m, Bolivia) [1, 2], Yang-bajing (4300m, China) [3, 8] and Tien-Shan (3340m, Kazakhstan) [4] for studying cosmic-ray nuclear interaction in the energy region around $10^{15} - 10^{17}$ eV. In the hybrid experiments, we can obtain the air-shower size, N_e , from the air-shower array data, particle-density, n_b , which are closely connected to the hadron component in the air-shower, from the hadron calorimeter (burst detector) and energy and geometrical position of individual high energy electromagnetic particles by the emulsion chamber. Correlations between air-showers and accompanying families were studied so far in these three experiments by comparing experimental data and simulated data [12, 13]. In the present paper we show some results obtained by studying correlations between the hadron component (data of hadron calorimeters) and families observed by emulsion chamber which are considered to be very sensitive to the mechanism of cosmic-ray interactions, using data of the Chacaltaya hybrid experiment.

2. Short summary of the analysis on air-showers and accompanied families

The shower-size, N_e , dependence on the family energy and on the lateral spread of the showers in the air-shower-triggered families were studied in the three hybrid experiments at high mountains. In Ref.[13] we have shown that the average family energy normalized by associating air-shower size, $\Sigma E_\gamma/N_e$, of the events with $N_e \geq 10^7$ observed in these hybrid experiments agree more or less to those expected in the case of heavy-dominant composition of primary particles, as shown in Figure 1, though the difference in the

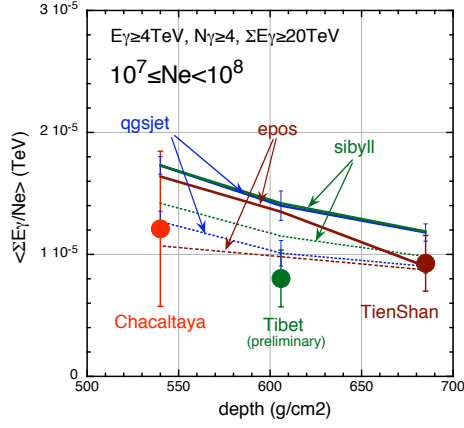


Figure 1: Depth dependence on the average family energy normalized by air-shower size for events with $10^7 \leq N_e < 10^8$. Solid lines are for proton-dominant composition and dotted lines for heavy-dominant composition [13].

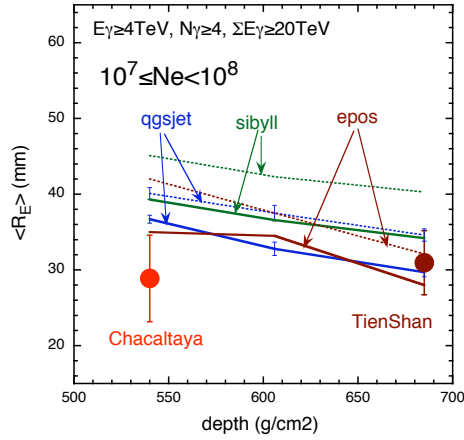


Figure 2: Depth dependence on the average lateral spread of EAS-triggered families with $10^7 \leq N_e < 10^8$ [13].

average value between the two chemical composition, proton-dominant and heavy-dominant, is not clear at the Tien-Shan altitude, especially in the case of the EPOS model. Some details of simulations are shown in Ref. [13]. The lateral spread of high energy showers in the families accompanied by the air-showers with $N_e \geq 10^7$ was also studied¹. The average lateral spread of showers in those families observed in the Chacaltaya experiment, shown in Figure 2, is found to be smaller than that expected in the case of a heavy-dominant composition. The difference in the average lateral spread between the two chemical compositions is again not clear in the Tien-Shan data. The Cha-

¹ There is no official publication about the lateral spread of families accompanied by air-showers in Tibet AS_{γ} experiments.

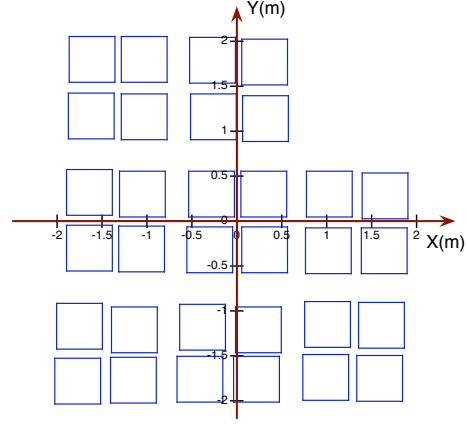


Figure 3: Configuration of 32 blocks of emulsion chambers and hadron calorimeters at the center of the Chacaltaya air-shower array.

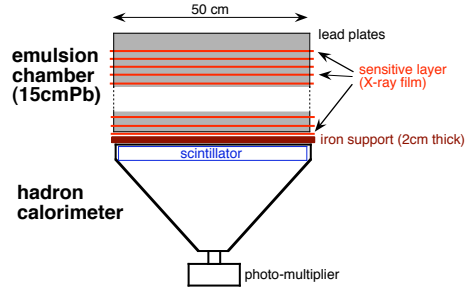


Figure 4: The structure (side view) of one of the blocks of the emulsion chamber and the hadron calorimeter (burst detector).

caltaya data show that the proton-dominant composition is favorable to explain the small lateral spread of the families but the heavy-dominant composition is favorable to explain small family energy. Thus the increase of heavier composition of primary cosmic rays alone can not explain the general characteristics of air-shower-triggered families, contrary to the results of the Tibet group and others [5, 8, 14].

The data of hadron calorimeters were also analyzed by the Chacaltaya and Tibet groups. The Tibet group concluded from the analysis that the experimental data were well explained by a heavy dominant composition of primary particles [3] but the Chacaltaya group concluded that the number of hadrons in the air-showers was less than expected [2].

3. Hybrid experiment at Mt.Chacaltaya

The air-shower array covers a circular area within a radius about 50 m by 35 plastic scintillation detectors to measure the lateral distribution of the electron

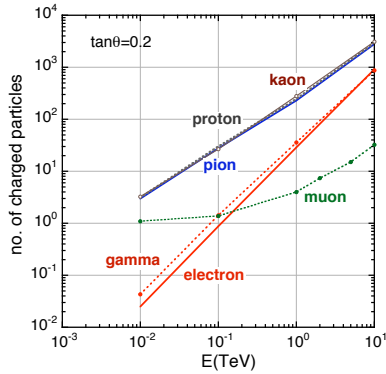


Figure 5: Energy dependence of average number of charged particles arriving to the scintillator of the hadron calorimeter for π^- , proton, K^- , μ^- , e^- and γ incidence.

density of the air-showers. In the center of the air-shower array, 32 blocks of emulsion chambers (0.25 m^2 each) are installed (see Figure 3). Each block of the emulsion chamber consists of 30 lead plates each of 0.5 cm thick and 14 sensitive layers of X-ray film which are inserted after every 1 cm lead. The total area of the emulsion chambers is 8 m^2 . Hadron calorimeters with plastic scintillator of 5cm thickness are installed underneath the respective blocks of the emulsion chamber (see Figure 4). An iron support of 2 cm thick is inserted between the emulsion chamber and the hadron calorimeter. Some detail of the Chacaltaya hybrid experiment are described in Refs.[1, 2]

4. Simulations

4.1. Air-showers and families

For generating extensive air-showers and families we use the CORSIKA simulation code (version 6.735) [15] employing the QGSJET model (QGSJET01c) [16] and the EPOS model (EPOS 1.60) [9, 10] for the cosmic-ray nuclear interaction. Primary particles of $E_0 \geq 10^{15} \text{ eV}$ are sampled respectively from the power law energy spectrum of integral power index -1.7 , for pure protons and pure iron, and also from the energy spectrum of primary cosmic rays with proton dominant and a heavy dominant chemical composition. Some details of the chemical composition are shown in Table 1. The thinning energy is fixed to be 1 GeV. Shower size, N_e , at the observation point is calculated using the NKG option in the simulation. The air-shower center is randomly sampled within an area of $\pm 2.5 \text{ m}$ in the X and Y directions from the center of the hadron detectors (see Figure 3).

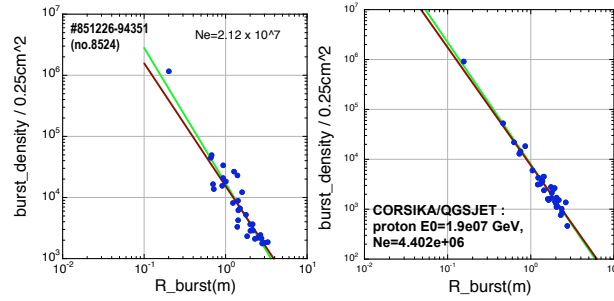


Figure 6: Examples of burst data in the form of the lateral distribution of burst-density for experimental data (left) and for simulated data of proton-primary (right).

4.2. High energy showers in emulsion chambers

For high energy (e, γ)-particles and hadrons of $E \geq 1 \text{ TeV}$ in the atmospheric families arriving at each emulsion chamber, we calculate further the nuclear and electromagnetic cascade development inside the chamber taking into account the exact structure of the emulsion chamber. We use the QGSJET model for hadron-Pb interactions and a code formulated by Okamoto and Shibata for electromagnetic cascades [19]. The electron number density under every 1cm Pb is transformed into spot darkness of the X-ray film. Then the energy of each shower is re-estimated from the shower transition on spot darkness by applying the procedure used in the experiments.

4.3. Data of hadron calorimeters: Calculation of the burst-size

Hadron calorimeters detect a bundle of charged particles, which are produced in the emulsion chamber material by the hadron component in the air-shower through local nuclear interactions. Output from each unit of the hadron calorimeter is related to the energy deposited in the scintillator, and is converted to a charged particle number using the average energy loss of a single muon in the scintillator. The number of charged particles per $50 \text{ cm} \times 50 \text{ cm}$, n_b , is called the “burst density” hereafter. We use the GEANT4 code [20] for calculating the burst-density. We calculate the average number of charged particles² produced in the emulsion chamber of 15 cmPb and arriving at the scintillator of the hadron calorimeter for hadrons (pions, proton, kaons), muons and high energy e, γ in the air-shower, with 4 different energies

² Here we take into account the scintillator response of charged particles. Gamma-rays gives some energy deposit in the scintillator. Then the scintillator response of gamma-rays are also taken into account[21].

Table I Chemical composition of primary cosmic-rays and air-showers

E_0 (eV)	sampled primary particles									
	proton dominant					heavy dominant				
	protons	He	CNO	heavy	Fe	protons	He	CNO	heavy	Fe
$10^{15} - 10^{16}$	42 %	16 %	16 %	14 %	12 %	17 %	10 %	18 %	15 %	40 %
$10^{16} - 10^{17}$	42 %	12 %	13 %	15 %	18 %	14 %	8 %	17 %	14 %	47 %
air-showers accompanied by burst (CORSIKA/QGSJET)										
	protons	He	CNO	heavy	Fe	protons	He	CNO	heavy	Fe
$10^6 < N_e < 10^7$	57 %	18 %	11 %	9 %	5 %	31 %	13 %	11 %	13 %	26 %
$10^7 < N_e < 10^8$	46 %	11 %	13 %	11 %	18 %	16 %	12 %	21 %	9 %	42 %
air-showers accompanied by families of $\Sigma E_\gamma \geq 10$ TeV (CORSIKA/QGSJET)										
	protons	He	CNO	heavy	Fe	protons	He	CNO	heavy	Fe
$10^6 < N_e < 10^7$	70 %	19 %	6 %	4 %	2 %	48 %	17 %	17 %	8 %	10 %
$10^7 < N_e < 10^8$	50 %	9 %	14 %	7 %	20 %	23 %	10 %	19 %	3 %	45 %

of 10 GeV, 100 GeV, 1 TeV and 10 TeV and 5 different zenith angles of arrival direction. Figure 5 shows an example of the energy dependence of average number of charged particles which responds to scintillator for six different incident particles. The dependences are approximated by numerical functions and extrapolate to higher or lower energy range of the incident particles. Applying these functions to every particle incident upon the emulsion chamber, we get the burst-density in each block of 32 hadron calorimeters. We define n_b^{max} as the largest burst-density among the 32 blocks of the hadron calorimeters and Σn_b as the sum of burst-density of 32 blocks. In the following we pick up events which satisfy the following criteria;

- $N_e \geq 10^6$,
- $n_b^{max} \geq 10^4$,
- $R_{AS-Bs} \leq 1\text{m}$,
where R_{AS-Bs} is the distance between the burst center and the air-shower center.

The burst center is determined by the algorithm described in Ref.[2]. In the Chacaltaya data, 1,034 events satisfy the above criteria in $\sim 40 \text{ m}^2\text{year}$ exposure of hadron calorimeters. Among them, 73 events are accompanied by high energy atmospheric families of $\Sigma E_\gamma \geq 10 \text{ TeV}$ ($E_{min} = 2 \text{ TeV}$). Figure 6 show examples of experimental and simulated burst data. We can see the lateral distribution of the burst-density is well described by the power law function [2].

In Table 1, we show the fraction of proton, He, CNO, heavy and Fe components in the air-showers accompanied by families and also those accompanied by burst. In the shower-size region of $N_e \geq 10^7$, corresponding to $E_0 \approx 10^{16} - 10^{17} \text{ eV}$, the fraction of each component is similar to those assumed in the primary particles because almost all air-showers in this air-shower size region accompany families and bursts.

5. Correlation between air-showers and bursts

Figure 7 shows a scatter diagram between air-shower size, N_e , and maximum burst density, n_b^{max} , of the event for the experimental data and for the simulated data of proton- and Fe-primaries. In the events of iron-primaries, n_b^{max} is more or less proportional to N_e though n_b^{max} is weakly correlated to N_e for the events of proton primaries. It is very natural because Fe-air-nucleus interactions are assumed to be the superposition of a number of low energy nucleon-air-nucleus collisions and so the fluctuation becomes small. But for proton-air-nucleus interactions, the position of interactions and/or released energy at the interaction fluctuate widely event by event. The distribution in the experimental data looks close to that in proton-primaries. Figure 8 shows distributions of n_b^{max}/N_e for four different chemical composition of primary particles, pure proton, pure iron, proton-dominant and heavy dominant. The shape of the distribution for pure-iron primaries is very different from that for the others. There are almost no events with $n_b^{max}/N_e \gtrsim 0.02$ ($\log(n_b^{max}/N_e) \gtrsim -1.6$) in the iron-induced air-showers. On the contrary, a considerable number of events are found in this region of the distribution for proton-induced air-showers. There is no systematic difference in the shape for the other three chemical compositions, pure protons, proton-dominant and heavy dominant³, and also for the two different interaction models, QGSJET and EPOS. The experimental data are well described by

³ Nearly half of the air-showers accompanied by bursts are due to protons and He-nuclei, even when heavy-dominant chemical composition is assumed in primary particles, as seen in Table 1. This is a reason why the difference in the shape of the distribution among these three chemical compositions is small.

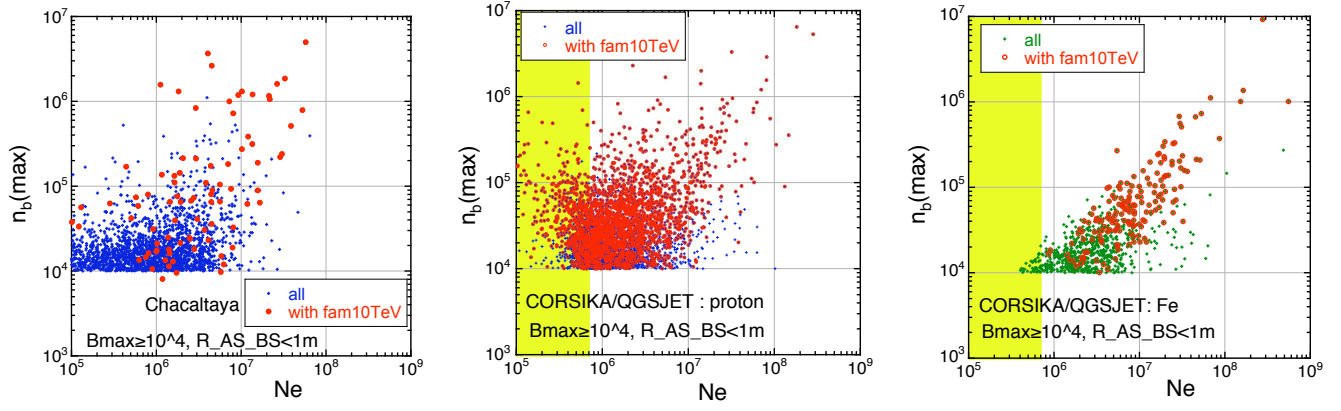


Figure 7: Scatter diagram between air-shower size, N_e , and maximum burst density, n_b^{max} , of the event. Shaded area in the simulated data is biased because the sampled primary energy is larger than 10^{15} eV.

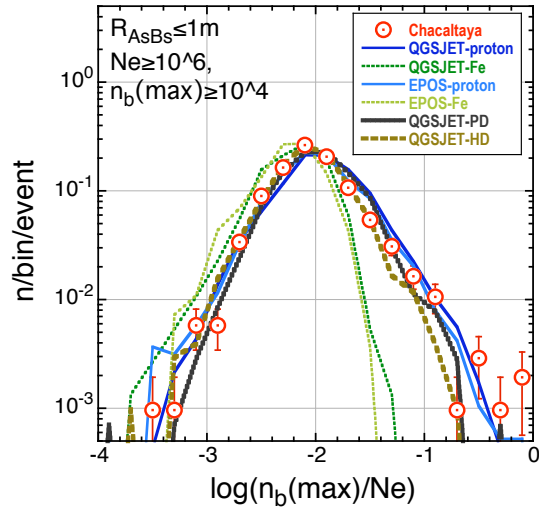


Figure 8: Distribution of n_b^{max}/N_e . Circles are experimental data and lines are simulated data, solid lines : proton-primaries, dotted lines : Fe-primaries.

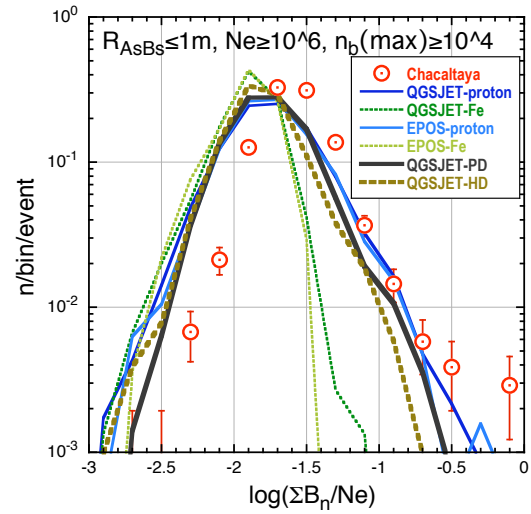


Figure 9: Distribution of $\Sigma n_b/N_e$. Circles are experimental data and lines are simulated data, solid lines : proton-primaries, dotted lines : Fe-primaries.

the model calculation for these three chemical compositions of primary particles. Figure 9 shows the distribution of $\Sigma n_b/N_e$ where Σn_b is a sum of n_b over 32 blocks of hadron calorimeters. Again we can see the experimental data are close to those expected for pure protons or mixed chemical composition of proton-dominant and heavy-dominant, though the number of events with smaller Σn_b are less than expectation. An almost similar analysis was done by the Tibet group and they concluded that their data are well described by a heavy dominant composition (see Ref.[3]).

6. Correlation between bursts and families

Figure 10 shows a correlation diagram between n_b^{max} , maximum of burst size among 32 blocks of the event and accompanying family energy. The experimental data are compared with those of simulated data of proton-primaries and iron-primaries. As seen in the figure, the family energy is almost proportional to n_b^{max} in the simulated data irrespective of the primary particles though the family energy of the events coming from iron-primaries are smaller than that from proton-primaries. In the figure we can see the family energy in the experimental data is systematically smaller than that of simulated data in the events with larger burst-density, $n_b^{max} \geq 10^5$. Figure 11 shows an average family energy versus n_b^{max} . It is clear that

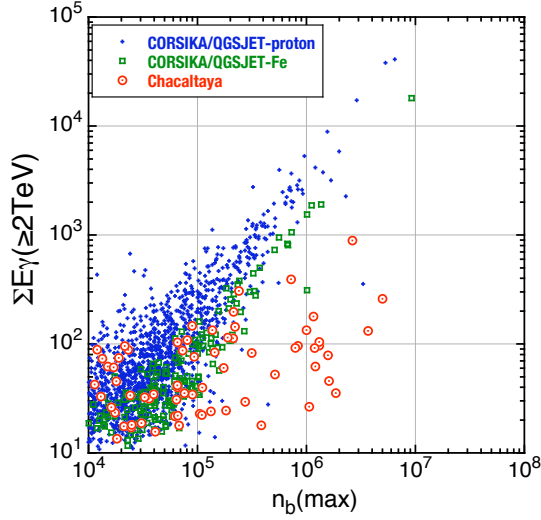


Figure 10: Correlation diagram between n_b^{max} and family energy ΣE_γ in the burst-triggered families in the air-showers of $N_e \geq 10^6$.

the experimental data can not be explained simply by changing the chemical composition of primary particles.

One may argue that the smaller family energy in the experimental data is due to the systematic underestimation of the shower energy in the emulsion chamber. Figure 12 shows a comparison of the integral spectra of family energy observed by the present hybrid experiment and that by the emulsion chamber experiment of the Brazil-Japan collaboration[22]. As seen in the figure, the two spectra smoothly connect with each other. Thus we can conclude that the energy estimation of high energy particles in the emulsion chamber of the present hybrid experiment is not much different from that of the emulsion chamber experiment of the Brazil-Japan collaboration.

One may also argue about an overestimation of the burst-density, especially beyond the region of $n_b \geq 10^5$. But this possibility is also ruled out, because the distribution on n_b^{max}/N_e is well described by the simulations as seen in Figure 8.

7. Discussion

The previous analysis on the air-shower-triggered families shows that the average family energy of the experimental data is considerably smaller than that of simulations of proton-dominant primaries in the shower size region of $N_e \geq 10^7$, as described in section 2. In Figure 13 we show a correlation diagram between family energy, ΣE_γ and associated air-shower size, N_e , for the same events shown in Fig.10. In the air-shower-size region of $N_e \geq 10^7$, the family energy in the experimental data is systematically smaller than that

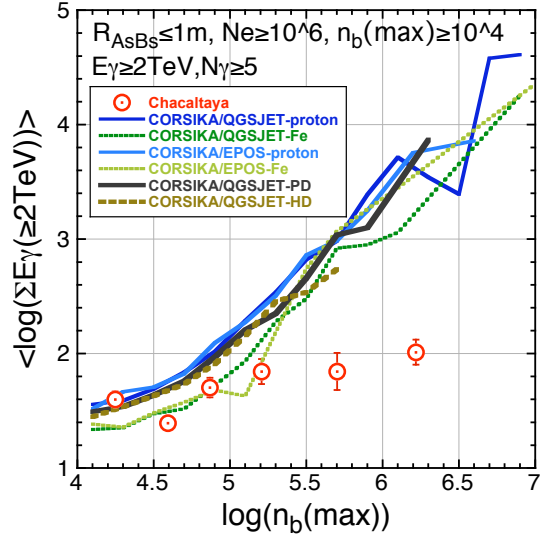


Figure 11: Average family energy versus n_b^{max} in the burst-triggered families.

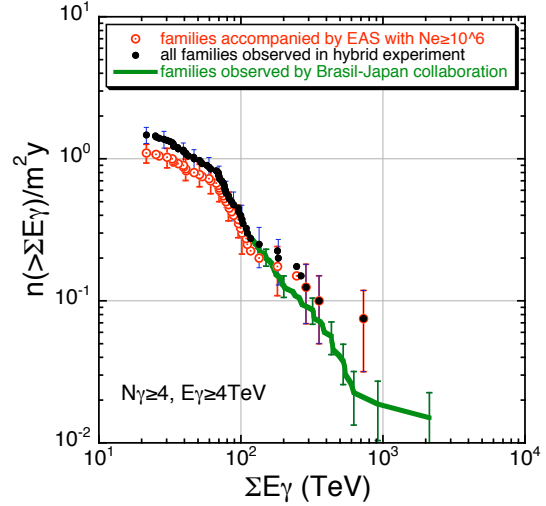


Figure 12: Comparison of the integral family energy. The solid line is for the emulsion chamber experiment of the Brazil-Japan Collaboration and solid circles are for air-shower triggered families and open circles are for all families observed in the present hybrid experiment.

expected for proton-primaries and those events look like coming from iron-primaries.

The characteristics of the bursts accompanied by the proton-induced air-showers are very different from those accompanied by iron-induced ones, as shown in Figure 7. The considerable number of air-showers induced by proton-primaries accompany large burst-density which are not seen in the iron-induced air-showers, and the experimental data are close to those expected in case of proton-primaries. The contradiction of the above two arguments is well seen in the

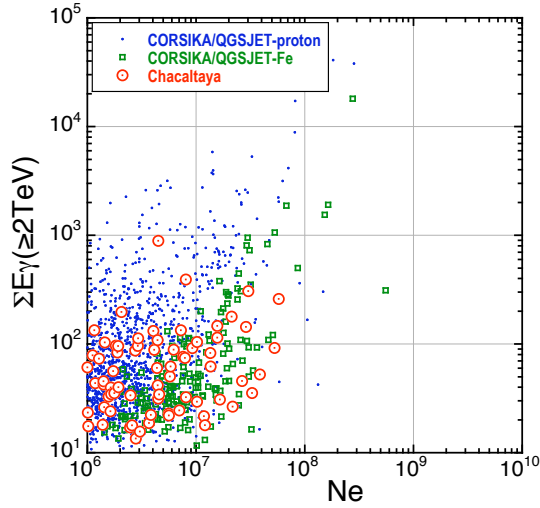


Figure 13: Correlation diagram between air-shower size, N_e , and accompanied family energy, ΣE_γ , of the events shown in Figure 10.

correlation diagram between bursts and families, shown in Figure 10 and no model can describe the observed correlation.

The spectra of high energy particles detected by the emulsion chambers are more sensitive to the mechanism of the particle production of the most forward region of the rapidity. The hadron calorimeter supplies the data of hadron component in the air-shower. The hadron component in the air-shower bears more direct information on the nuclear interaction than any other component such as electron and muon component in the air-shower, and the burst-size of hadron calorimeter gives a measure of interaction energy.

Suppose the x -distribution of the produced particles becomes steeper, the number of high energy particles detected in the emulsion chamber becomes small (i.e., detected family energy becomes smaller), because of the high threshold energy of the emulsion chambers. The hadron component detected by hadron calorimeters, however, does not change much because of the lower detection threshold energy. Then the ration of $\Sigma E_\gamma / n_b^{max}$ becomes smaller. The observed discrepancy between experimental data and simulated data can be explain in this way, that is, the experimental data indicate the x -distribution of produced particles in the cosmic-ray nuclear interactions of $E_0 \gtrsim 10^{16}$ eV is much steeper than that assumed in the models.

Acknowledgments

The author wishes to thank all the member of Chacaltaya hybrid experiment, especially to Drs. N.Kawasumi, K.Honda, N.Ohmori, N.Inoue and A.Ohsawa for their valuable comments and discussions on the details of experimental procedures.

References

- [1] N.Kawasumi et al., Phys. Rev. D **53** (1996) 3534
- [2] C.Aguirre et al., Phys. Rev. D **62** (2000) 032003
- [3] Tibet AS γ Collaboration (M.Amenomori et al.), Phys. Rev. D **62** (2000) 112002-1, 072007-3
- [4] S.B.Shaulov, AIP Conf. Proc. **276** (1992) 94
- [5] Y.Shirasaki et al., Astropart. Phys. **15** (2001) 357
- [6] T.Antoni et al. KASCADE Collaboration, Astropart. Phys. **14** (2001) 245, **19** (2003) 703,715
- [7] S.P.Swordy et al., Astrop. Phys. **18** (2002) 129
- [8] Tibet AS γ Collaboration (M.Amenomori et al.), Phys. Lett. B **632** (2006) 58
- [9] K.Werner, F.M.Liu and T.Pierog, Phys. Rev. C **74** (2006) 044902
- [10] T.Pierog and K.Werner, Proceedings of 30th ICRC, Merida (2007), Vol.4, p.629
- [11] H.Urlich et al., Proceedings of 30th ICRC, Merida (2007), Vol.4, p.87
- [12] H.Aoki et al., Proceedings of 30th ICRC, Merida (2007), Vol.4, p.23
- [13] S.P.Besshapov et al., Nucl. Phys. B (Proc. Suppl.) **196**(2009) 118; Proceedings of 31th ICRC, Lodz (2009) #0214
- [14] J.R.Horandel, Astropart. Phys. **19** (2003) 193
- [15] D.Heck, J.Knapp, J.N.Capdevielle, G.Schatz and T.Thouw, Fortshungzentrum Karlsruhe, FZKA 6019 (1998)
- [16] N.N.Kalmykov and S.S.Ostapchenko, Yad. Fiz. **56** (1993) 105
- [17] R.S.Fletcher et al., Phys. Rev. **D50** (1994) 5710
- [18] J.Engel et al., Phys. Rev. **D46** (1992) 5013,
- [19] M.Okamoto and T.Shibata, Nucl. Instr. and Meth. A **257** (1987) 155
- [20] S.Agostinelli et al. Geant4 collaboration, Nucl. Inst. and Meth. A **506**(2003) 250
- [21] N.Ohmori, private communication.
- [22] C.M.G.Lattes, Y.Fujimoto and S.Hasegawa, Phys. Rep. Vol.65 (1980) 151